LETTER • OPEN ACCESS

Widespread deepening of the active layer in northern permafrost regions from 2003 to 2020

View the article online for updates and enhancements.

ENVIRONMENTAL RESEARCH
LETTERS

CrossMark

Widespread deepening of the active layer in northern permafrost regions from 2003 to 2020

Zhihua Liu[1,*] ⓘ, John S Kimball[1], Ashley Ballantyne[2], Jennifer D Watts[3], Susan M Natali[3],
Brendan M Rogers[3], Yonghong Yi[4], Anna E Klene[2], Mahta Moghaddam[5], Jinyang Du[1]
and Donatella Zona[6,7] ⓘ

[1] Numerical Terradynamic Simulation Group, WA Franke College of Forestry and Conservation, University of Montana, Missoula, MT, United States of America
[2] Department of Ecosystem and Conservation Sciences, WA Franke College of Forestry and Conservation, University of Montana, Missoula, MT, United States of America
[3] Woodwell Climate Research Center, Falmouth, MA, United States of America
[4] College of Surveying and Geo-Informatics, Tongji University, Shanghai 200092, People's Republic of China
[5] Ming Hsieh Department of Electrical and Computer Engineering, University of Southern California, Los Angeles, CA 90089, United States of America
[6] Department of Biology, San Diego State University, 5500 Campanile Drive, San Diego, CA 92182, United States of America
[7] School of Biosciences, University of Sheffield, Sheffield, United Kingdom
* Author to whom any correspondence should be addressed.

E-mail: liuzh811@126.com

Abstract

The changing thermal state of permafrost is an important indicator of climate change in northern high latitude ecosystems. The seasonally thawed soil active layer thickness (ALT) overlying permafrost may be deepening as a consequence of enhanced polar warming and widespread permafrost thaw in northern permafrost regions (NPRs). The associated increase in ALT may have cascading effects on ecological and hydrological processes that impact climate feedback. However, past NPR studies have only provided a limited understanding of the spatially continuous patterns and trends of ALT due to a lack of long-term high spatial resolution ALT data across the NPR. Using a suite of observational biophysical variables and machine learning (ML) techniques trained with available *in situ* ALT network measurements ($n = 2966$ site-years), we produced annual estimates of ALT at 1 km resolution over the NPR from 2003 to 2020. Our ML-derived ALT dataset showed high accuracy ($R^2 = 0.97$) and low bias when compared with *in situ* ALT observations. We found the ALT distribution to be most strongly affected by local soil properties, followed by topographic elevation and land surface temperatures. Pair-wise site-level evaluation between our data-driven ALT with Circumpolar Active Layer Monitoring data indicated that about 80% of sites had a deepening ALT trend from 2003 to 2020. Based on our long-term gridded ALT data, about 65% of the NPR showed a deepening ALT trend, while the entire NPR showed a mean deepening trend of 0.11 ± 0.35 cm yr^{-1} [25%–75% quantile: $(-0.035, 0.204)$ cm yr^{-1}]. The estimated ALT trends were also sensitive to fire disturbance. Our new gridded ALT product provides an observationally constrained, updated understanding of the progression of thawing and the thermal state of permafrost in the NPR, as well as the underlying environmental drivers of these trends.

1. Introduction

Permafrost, defined as ground that remains at or below 0 °C for at least two consecutive years, covers around 16×10^6 km^2 (~12%) of Earth's land area and is primarily distributed in high latitude and altitude regions of the Northern Hemisphere (Zhang *et al* 2000, Obu 2021). The active layer is the near-surface layer of soil or rock that thaws and freezes seasonally on top of permafrost. The active

layer affects the amount of water and heat exchange between the land surface and atmosphere, and the ecosystem that can be supported, and is therefore a key component of the cryosphere (Heijmans *et al* 2022). As the climate warms, thawing permafrost will increase the active layer thickness (ALT), potentially mobilizing and releasing vast amounts of soil organic carbon (SOC) sequestered over millennia in permafrost soils. The enhanced decomposition and atmospheric release of SOC in the form of carbon dioxide (CO_2), methane (CH_4), and other radiatively active greenhouse gases could drive a positive feedback between permafrost thaw and climate warming (Schuur *et al* 2015, 2022, Miner *et al* 2022). Concurrently, increases in ALT allow for increased rooting depth of vegetation that may lead to changes in the distribution and productivity of vegetation at high latitudes and altitudes (Song *et al* 2018, Berner *et al* 2020). Therefore, improved understanding of the spatial pattern and rates of active layer deepening, and the environmental factors influencing ALT heterogeneity, is needed to better understand the nature of permafrost-climate feedbacks affecting the rate of global warming (McGuire *et al* 2018), and the consequences for northern ecosystems and communities.

Regional assessments based on sparse inventory and monitoring networks indicate that the ALT varies greatly across northern permafrost regions (NPRs), ranging from about 30 cm in Arctic and subarctic regions to over 10 m in mountainous permafrost regions at mid-latitudes, and that this pattern is broadly consistent with surface air temperature and permafrost gradients (Luo *et al* 2016). Based on *in situ* active layer monitoring networks, gridded ALT maps have been produced using various up-scaling techniques (Ran *et al* 2022) and modeling (Obu *et al* 2019). While these gridded ALT maps have greater congruence in densely monitored regions, such as Alaska and northwest Canada, there are large uncertainties in more sparsely monitored regions, such as Siberia and high-elevation regions like Mongolia and the Tibetan Plateau. In addition, most current hemispheric ALT maps are produced either based on coarse climate indicators (i.e. thaw index), or modeling; thus, there is a need to better understand finer-scale variation of ALT using observationally constrained approaches in the NPR.

While there is considerable ALT variability, the nature of the ALT spatial distribution and underlying environmental drivers are uncertain due to the vast size and complexity of NPR landscapes, and relative paucity of regional monitoring sites. ALT temporal trends are even more difficult to observe because permafrost change is a subsurface phenomenon that is difficult to detect with remote-sensing techniques. However, current monitoring networks have allowed some regional and local-scale evaluations of ALT trends in North America (Smith *et al* 2005, Nyland

et al 2021), Siberia (Romanovsky *et al* 2007), Europe and Scandinavia (Harris *et al* 2003, 2009, Isaksen *et al* 2007), and the Tibetan Plateau (Wu and Zhang 2008). Long-term monitoring data from these limited studies indicates a predominantly deepening ALT trend in the Arctic since the 1990s, but with marked spatial variability (Smith *et al* 2022). The greatest increases have been recorded in the Russian European north and western Siberia with an average increase of 1.9 cm yr^{-1} between 1999 and 2019 (Romanovsky *et al* 2019). In the Alaskan interior, the rate of ALT increase is more than 0.83 cm yr^{-1} from 1996 to 2019 (Romanovsky *et al* 2019). However, in the Alaskan North Slope and Mackenzie Valley, the trends have been more inconsistent, with ALT decreasing after a 1998 peak, and then transitioning to a slight increase since the mid-2000s (Smith *et al* 2022). In northern Sweden, Norway, central Svalbard, and northeast Greenland, ALT has generally increased since the 1990s at an average rate similar to the Russian Arctic, but with considerable inter-annual variation (Zhao *et al* 2020) and some Swedish sites have reported permafrost loss (Åkerman and Johansson 2008). Pronounced increases in ALT have also been observed in the European Alps since the 1990s, with present-day rates of ALT increase typically greater than the global average. On the Tibetan Plateau, ALT has tended to increase at a much higher rate ($\sim$1.95 cm yr^{-1}) than high latitude permafrost regions since 1980 (Zhao *et al* 2020).

Recent development of upscaled long-term gridded ALT data have also allowed for the assessment of ALT trends encompassing the entire NPR. However, these studies have often employed a relatively simple thawing index-based Stefan model or edaphic factor (*E* factor) method based on very coarse climate ($\sim$0.5°) and land cover data. For example, Peng *et al* (2018) showed that mean ALT increased significantly by 0.057 $\pm$ 0.004 cm yr^{-1} during 1850–2005. Li *et al* (2022b) used the Kudryavtsev method and integrated various forcing data (such as temperature, snow, vegetation and soil data) to simulate changes in ALT in the NPR and found ALT increased at a linear rate of 0.86 cm yr^{-1} from 1969 to 2018, with the highest thickening rate in Alaska and the Mongolian Plateau ($\sim$2.4 cm yr^{-1}) and the lowest thickening rate in Greenland ($\sim$0.3 cm yr^{-1}). Li *et al* (2022a) reported an overall significant linear increase in ALT of 0.65 cm yr^{-1}, with approximately 71% of the NPR showing an increase from 2000 to 2018. These studies provide useful understanding of broad regional patterns and climate impacts on ALT trends, but are generally too coarse to resolve finer landscape heterogeneity, where local terrain, soil, and vegetation features may have a larger influence on permafrost stability.

Although many studies have investigated the spatial and temporal pattern of ALT over the NPR, some inherent uncertainties exist. First, the current

ALT monitoring network is spatially and temporally biased, making it hard to detect and compare long-term trends among different regions. Second, permafrost is a subsurface phenomenon and most available remote-sensing techniques are not directly sensitive to ALT and permafrost thermal states, especially at moderate to high spatial resolutions. Current assessments of regional ALT patterns generally use a thermal index based on air temperature derived indices (e.g. thawing index) at coarse resolution ($\sim$0.5°), and thus cannot reveal the local to landscape level patterns that are more relevant to ecological and hydrological processes. Therefore, there is a need to develop higher resolution, observationally constrained ALT datasets spanning the entire NPR to better understand ALT heterogeneity in relation to climate, land cover, and other environmental factors. The objectives of this study are to: (1) develop a consistent ALT data record encompassing the entire NPR and able to resolve landscape (1 km) level heterogeneity in active layer trends, and (2) apply these data to clarify ALT trends, driving factors and associated uncertainties over the recent satellite era (2003–2020). The ALT record is derived using a data-driven machine-learning (ML) framework informed by an extensive collection of ALT measurements and ALT-related observational indicators derived from the recent satellite record.

2. Materials and methods
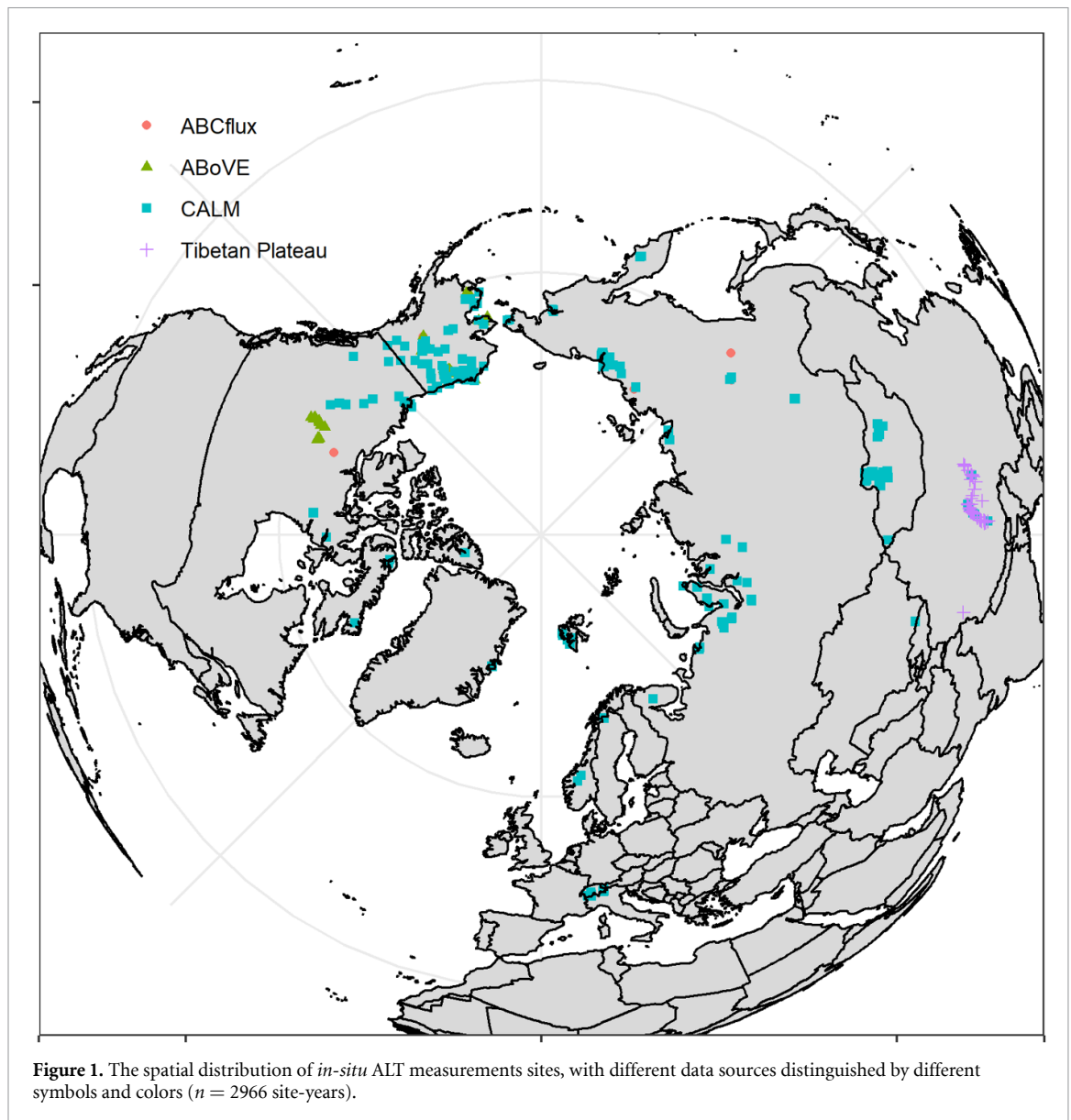
2.1. Overall study design

We utilized random forests (RFs) to generate a 1 km gridded annual ALT dataset from 2003 to 2020 in the NPR based on the relationship between available ALT site measurements (2966 site-years) and other supporting environmental and climate data in the NPR. We aggregated *in-situ* ALT measurements from four sources and used Google Earth Engine to compile satellite observations of annual gridded predictors, including vegetation, temperature, soil, and topography at 1 km resolution (Gorelick *et al* 2017). We created an RF training dataset by matching ALT and associated predictor variables both spatially and temporally, and selecting the top ten performing RF models. An annual ALT map for the NPR was generated using the ensemble mean of ALT from the ten best RF predictions. To understand the uncertainties from spatial sampling of ALT and RF parameter selections, we conducted an extensive uncertainty analysis. Finally, the spatial and temporal patterns, and uncertainties, of ALT from 2003 to 2020 were analyzed. We also evaluated whether the estimated ALT pattern was sensitive to fire history, which was not directly incorporated in the RF modeling, but can have an important influence on permafrost stability (Michaelides *et al* 2019, Li *et al* 2021).

2.2. *In-situ* ALT measurement data

We collected *in-situ* ALT measurement data from four different sources between 2003 and 2020, totaling 2966 site-years, including the Circumpolar Active Layer Monitoring Network (CALM, 2409 site-years; (Brown *et al* 2000, Nelson *et al* 2021), NASA Arctic Boreal Vulnerability Experiment (ABoVE) Soil Moisture and Active Layer Thickness (SMALT) data (257 site-years; (Clayton *et al* 2021), Arctic-boreal CO_2 flux (ABCflux) Database (142 site-years; (Virkkala *et al* 2022), and additional ALT measurements from the Tibetan Plateau (158 site-years; figure 1) (Zhao *et al* 2021, Wu *et al* 2022).

The CALM network is an international initiative that collects long-term, standardized ALT and permafrost-related variables at 265 sites since the 1990s. The CALM data are widely used to study and monitor regional ALT trends and are considered a valuable resource in the field of permafrost research. Details about the site characteristics, ALT measurement methods (primarily mechanical probing and some frost tubes), data processing, and standardization can be found at www2.gwu.edu and in (Brown *et al* 2000, Shiklomanov *et al* 2008), among others. The ABoVE SMALT dataset provides *in-situ* measurements of ALT, soil moisture (SM), and dielectric properties from boreal and tundra research sites in Alaska and the Northwest Territories in Canada. The data were collected between 2008 and 2020 and consist of 206 000 observations of ALT obtained through mechanical probing (6%) or ground penetrating radar (94%). The ALT observations were taken during the end of the thaw season in August and September and were first averaged among multiple observations per site and then among sites located within 1 km of each other. The ABCflux dataset contains a standardized monthly collection of terrestrial carbon fluxes and associated site variables for 244 sites in Arctic and boreal regions from 1989 to 2020. The data include soil properties such as soil temperature and ALT, as well as vegetation and disturbance type and micrometeorological conditions. We selected the sites and years with ALT collected near the end of the thaw season (e.g. August and September) for analysis. To supplement *in-situ* ALT measurements over the Tibetan Plateau, additional data were extracted from a series of published papers (Zhao *et al* 2021, Wu *et al* 2022). These data include long-term meteorological, ground temperature, SM, and soil temperature data, and have been quality-controlled from an integrated, distributed, and multiscale observation network in permafrost regions of the Tibetan Plateau.

All the compiled *in-situ* ALT measurements underwent screening and quality control to help ensure accuracy. Specifically, for each site, the ALT

Figure 1. The spatial distribution of *in-situ* ALT measurements sites, with different data sources distinguished by different symbols and colors ($n = 2966$ site-years).

distribution was visually checked, and extreme values were excluded if they were greater than 2 standard deviations (sd) from their long-term mean. The final ALT dataset has a mean value of 122 cm and a median value of 66 cm. Only data within the 1% to 99% quantile range (27–660 cm) were retained for analysis. These data were used for RF training of the NPR-domain ALT model that was used for generating the 1 km gridded ALT annual data record from 2003 to 2020 (figure 1). Sites with at least 10 years of continuous measurement ($n = 57$) were used for site-level trend comparison. The *in-situ* ALT measurements were spatially and temporally matched with gridded environmental predictors (table 1) to create the training dataset for RF modeling (described in section 2.4.1 RF models).

2.3. Satellite and other gridded environmental predictors

We compiled a suite of satellite observations of annual gridded predictors, including vegetation, temperature, soil, and topography data, to estimate annual ALT from 2003 to 2020 over a 1 km NPR grid. All data sets were resampled to a consistent 1 km (0.0083°) resolution modeling grid (continuous rasters interpolated using bilinear interpolation and discontinuous rasters using nearest neighbor methods), projected to the World Geodetic System (WGS) 1984 projection and masked by permafrost extent (table 1). Data extraction and predictions were made over the 1 km^2 resolution model grid. All model predictors and subsequent ALT mapping and analysis were confined to a regional domain defined from an ancillary permafrost map from the International Permafrost

Table 1. Predictor variables used for RF ALT modeling.

Variables	Descriptions	Data source and native resolution
Annual thaw index (ATI)	$\text{ATI} = \sum_{day=1}^{n} \text{LST}_{avg}$ (only $\text{LST}_{avg} > 0$)Daily LST_{avg} is the average of daily gap-filled 1 km MODIS LST_{day} and LST_{night}	MODIS land surface temperature (LST) (MYD11A1.006, 1 km), updated annual from 2003 to 2020
Mean daily temperature (MDT)	Daily LST_{avg} is the average of daily gap-filled 1 km MODIS LST_{day} and LST_{night}	MODIS land surface temperature, (MYD11A1.006, 1 km), updated annual from 2003 to 2020
Percent tree cover	Percent of tree cover for each 1 km grid	MODIS vegetation continuous fields (MOD44B.006, 250 m), updated annual from 2003 to 2020
Summer maximum NDVI	Max NDVI for June, July, and August for each 1 km grid	MODIS Vegetation indices (MOD13A2.006), updated annual from 2003 to 2020
Percent surface water	Percent of surface water for each 1 km grid	Global surface water data (30 m), updated annual from 2003 to 2020
Freeze/thaw timing	Day of year for spring thaw and fall freeze	AMSR daily freeze/thaw record (6 km polar-grid), updated annual from 2003 to 2020
Snow phenology	Last day of spring snow off and first day of fall snow	IMS daily snow cover (4 km), updated annual from 2003 to 2020
Soil organic content (SOC)	Averaged 0–3 m SOC for each 1 km grid	SoilGrids (v2.0, 250 m), time invariant
Soil bulk density	Averaged 0–3 soil bulk density for each 1 km grid	
Soil texture	Percent of sand, clay, and silt content	
Land cover	Primarily based on MODIS IGBP land cover, and tundra classes were added	MODIS land cover (MCD12Q1.006, 1 km) and terrestrial ecoregion map, time invariant
Elevation	Elevation (m) representing altitudinal gradient in climate and active layer conditions	DEM (1 km), time invariant
Aspect	Southness (-1, 1), higher value receives more potential solar radiation	DEM (1 km), time invariant
Slope	Slope (degrees)	DEM (1 km), time invariant
Soil moisture	Summer (JJA) soil moisture ($m^3\ m^{-3}$)	ESA Climate Change Initiative(CCI) daily surface soil moisture (0–5 cm depth, 25 km), updated annual from 2003 to 2020
Latitude	Latitude (degrees) representing the poleward gradient in permafrost distribution	Time invariant

Association (Brown *et al* 1997) and further refined by the European Space Agency's permafrost extent map (Obu *et al* 2019). Detailed description about the data source and processing step can be found in the supplementary text.

2.4. Geospatial modeling of annual ALT
2.4.1. RF models
To train NPR-domain models of ALT, we utilized the R package h2o (LeDell and Poirier 2020) to run a series of RF ML models. We employed a grid-search approach to explore the results of multiple RF models, trained on *in-situ* ALT measurements using relevant geospatial data (table 1) as model predictors. The grid-search procedure involved selecting a list of hyperparameters, which varied in terms of the number of RF trees (*nt*, 50, 100, or 150), the number of variables sampled at each split (*nv*, 2–10), and the minimum observations per leaf (*no_leaf*, 2–5). In total, 108 models were generated for NPR ALT predictions. We evaluated the performance of each model using random tenfold cross-validation. We used coefficient-of-determination values (R^2) to
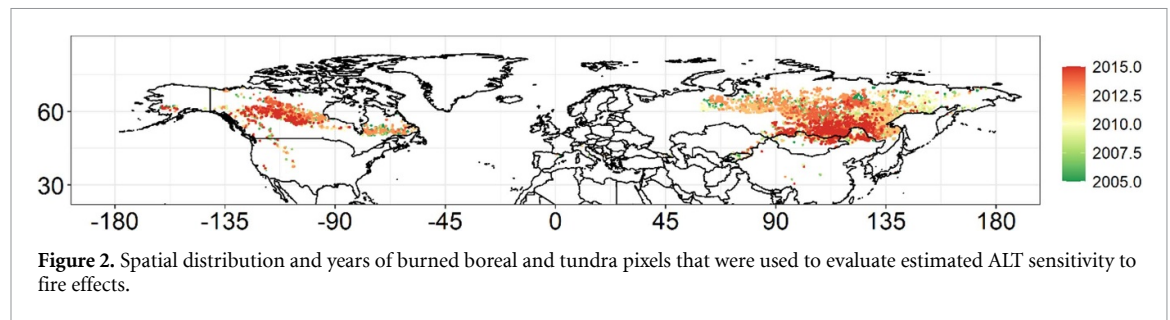
compute mean and sd for each cross-validated model. We selected the ten best models for ALT based on the highest mean R^2 values.

To create the final annual ALT maps at 1 km resolution, we used an ensemble approach, whereby for each year of record, we averaged the global predictions from the best ten RF models. By taking the average prediction across multiple models, ensemble methods minimize the influence of any single prediction, thereby stabilizing variation and minimizing bias that can otherwise arise from extrapolation or overfitting when using a single ML model (Sagi and Rokach 2018).

2.4.2. Uncertainty analysis
We conducted a series of uncertainty analyses to understand the effects of spatial bias in sampling and model structure (i.e. variation in *nt, nv*, and *no_leaf*), among other factors, potentially influencing the RF estimated ALT spatial pattern and trend.

To evaluate the effects of spatial bias in sampling on the ALT mean and trend, we performed a stratified

Figure 2. Spatial distribution and years of burned boreal and tundra pixels that were used to evaluate estimated ALT sensitivity to fire effects.

bootstrapping procedure. We set the number of bootstrap iterations to 100, that is, repeating the RF models (see section 2.4.1) 100 times and randomly selecting 75% of *in-situ* ALT measurements with replacement for each iteration. Each of the 100 bootstrap samples were used to produce annually resolved ALT maps from 2003 to 2020 using the method described above (section 2.4.1). The RF procedure resulted in a stack of ALT mean ($n = 100$) and trend ($n = 100$) map predictions from 2003 to 2020. Finally, these 100 images of mean and trend ALT maps were used to calculate per-pixel coefficient-of-variation values (sd divided by the mean predicted value) as a measure of spatial sampling uncertainty (figures S1 and S2).

To evaluate the effects of model structural uncertainty on the mean and trends in ALT, we first randomly selected one prediction out of the ten best performing RF models for each year ($n = 10$) from 2003 to 2020 ($n = 18$ years), which resulted in a total of 1800 total possible combinations of time-series gridded ALT maps. Then, we randomly selected 100 combinations, and calculated a stack of predicted ALT mean ($n = 100$) and trend ($n = 100$) layers from 2003 to 2020. Similarly, these 100 images of mean and trend ALT were used to calculate per-pixel coefficient-of-variation values (sd divided by the mean predicted value) as a measure of model structure uncertainty (figures S1 and S2).

Finally, we combined the mean ALT layers from above ($n = 200$, 100 from the spatial sampling and 100 from the model structure) and calculated the spatial patterns of mean, sd, coefficient of variation, and latitudinal summary of mean ALT from 2003 to 2020 (figure 4). We combined the resulting ALT trend layers and calculated the spatial patterns of the ensemble mean, lower prediction (ensemble of 2.5% quantile), (c) higher prediction (ensemble of 97.5% quantile), sd, and latitudinal summary of the ALT trend from 2003 to 2020 (figure 5).

2.4.3. Environmental drivers of ALT mean and trend
We utilized the RF models to determine the relative importance of each predictor variable in estimating the mean and trend of ALT (Breiman 2001). Additionally, we used partial dependence plots based on RF to visualize the relationship between predictor

variables and the mean and trend of ALT, while holding other predictor variables constant. This allows us to observe the marginal effect of individual predictor variables on the mean and trend of ALT, rather than the absolute value of changes. Predictor variables that have a flat response function, indicating no change in the mean and trend of ALT for a given predictor variable, are typically considered less important.

2.5. Evaluations of fire effects on ALT
Wildfire can have a significant impact on ALT in permafrost regions (Holloway *et al* 2020). Wildfires can increase the surface temperature and reduce insulating vegetation and soil organic layers, leading to thawing of permafrost and an increase in ALT. The increased thawing from fire can cause ground subsidence, particularly in ice rich permafrost, which can alter the hydrology and thermal balance, further affecting ALT. To assess whether our ALT predictions are sensitive to fire effects, we selected 50 000 burned pixels at 1 km spatial resolution between 2005 and 2015 using the MODIS burned area product (MCD64A1 v6, figure 2) and calculated the pre- and post-fire ALT change for different land cover types from the ALT annual time series.

3. Results and discussion

3.1. Spatial and temporal patterns of ALT
The cross-validation analysis indicated that the ensemble means of the ten best RF models achieved high accuracy for the ALT prediction (RMSE $= 21.60$ cm, bias $= 4.02$ cm, $R^2 = 0.97$, figure 3(a)). Site-level paired comparisons indicated that the RF-derived ALT captured the predominant deepening trends of ALT represented from CALM site measurements ($>80\%$, figure 3(d)). However, the RF-derived ALT data estimated a slower temporal trend of ALT deepening compared to the *in-situ* measurements at the higher range of observed ALT trends (e.g. trend >1 cm yr^{-1}, figure 3(e)). Generally, the RF-derived ALT data produced higher accuracy for mean ALT than for ALT trends, suggesting the ML approach is more capable of producing central tendency than temporal trend magnitude (see section 2.4.2).
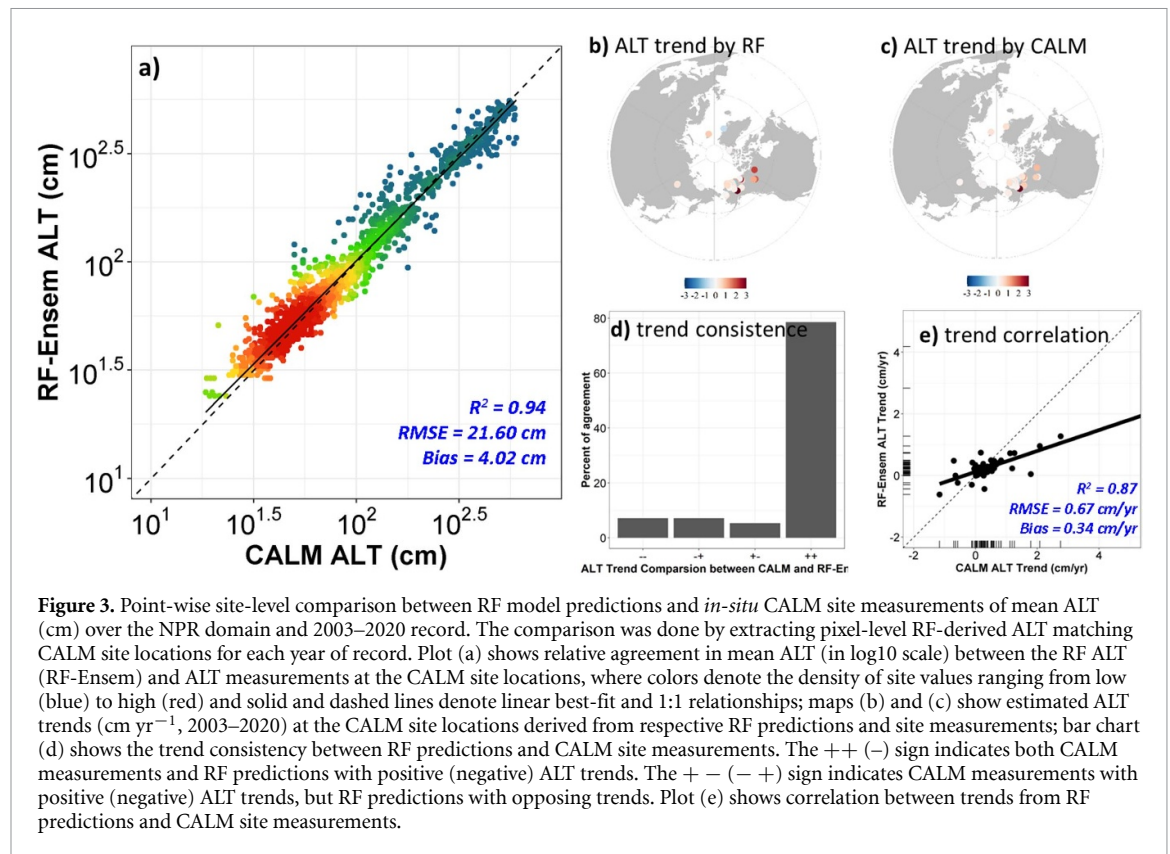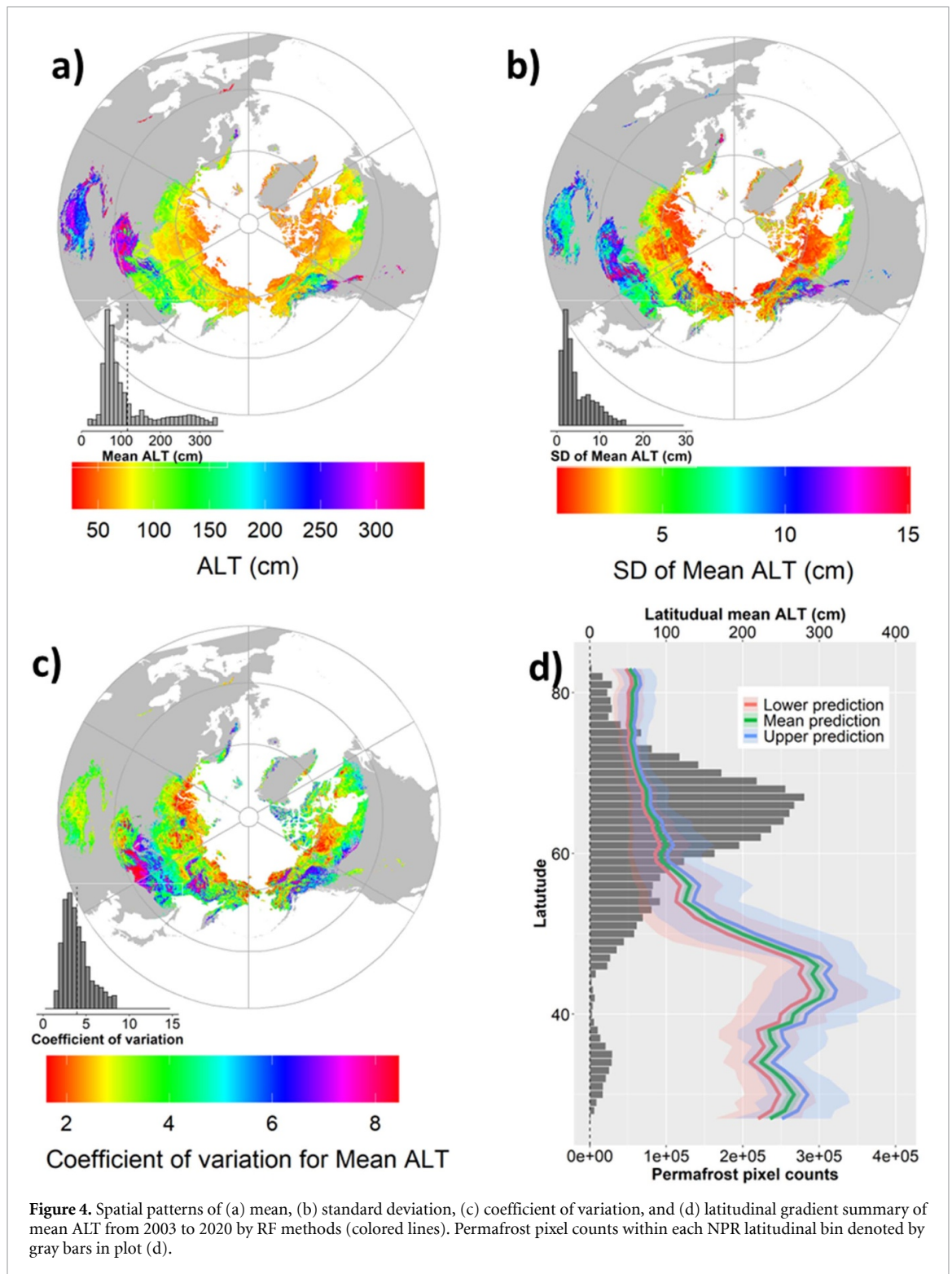
Figure 3. Point-wise site-level comparison between RF model predictions and *in-situ* CALM site measurements of mean ALT (cm) over the NPR domain and 2003–2020 record. The comparison was done by extracting pixel-level RF-derived ALT matching CALM site locations for each year of record. Plot (a) shows relative agreement in mean ALT (in log10 scale) between the RF ALT (RF-Ensem) and ALT measurements at the CALM site locations, where colors denote the density of site values ranging from low (blue) to high (red) and solid and dashed lines denote linear best-fit and 1:1 relationships; maps (b) and (c) show estimated ALT trends (cm yr^{-1}, 2003–2020) at the CALM site locations derived from respective RF predictions and site measurements; bar chart (d) shows the trend consistency between RF predictions and CALM site measurements. The $++$ $(-)$ sign indicates both CALM measurements and RF predictions with positive (negative) ALT trends. The $+-$ $(-+)$ sign indicates CALM measurements with positive (negative) ALT trends, but RF predictions with opposing trends. Plot (e) shows correlation between trends from RF predictions and CALM site measurements.

Based on the ensemble RF-derived ALT data from 2003 to 2020, we analyzed the distribution characteristics of the mean and trends of ALT in the NPR. The spatial patterns of mean ALT from 2003 to 2020 revealed large landscape level variations, highlighting that coarse resolution climate-based ALT assessments do not capture the full extent of spatial variability in ALT (figure 4). The distribution of mean ALT showed a bimodal pattern reflecting distinct latitudinal and elevational gradients within the NPR. Specifically, the mean ALT is 252.3 cm (25%–75% quantile: [219.2, 293.4]°cm) in the temperate zone (25–50°N), primarily in the Qinghai–Tibet and Mongolian plateaus. The ALT rapidly decreases to 87.8 cm (25%–75% quantile: [62.7, 94.7] cm) in the region poleward of 50°N latitude, corresponding to the main discontinuous to continuous permafrost regions in the NPR. The latitudinal patterns of mean ALT were similar among different percentages of permafrost extent and similar to a recent ML derived ALT map (Ran *et al* 2022) and the process-model based CCI ALT map (Obu *et al* 2021). However, there were some differences observed in the Qinghai–Tibet and Mongolian plateaus among the different datasets. Notably, the CCI ALT map underestimated ALT in temperate high-altitude regions, such as the Qinghai–Tibet and Mongolian plateaus, relative to this study and other sources (Ran *et al* 2022). The results of the uncertainty analyses showed that the RF-driven ALT maps have relatively small inter-model variations, with a mean sd of 4.1 cm (25%–75% quantile: [1.7,

5.2] cm), suggesting relative high accuracy in estimating mean ALT. Higher uncertainties are mainly located in high elevation regions, such as the Qinghai–Tibet and Mongolian plateaus. However, it should be noted that spatial sampling bias had a stronger influence on the mean ALT predictions than the RF model parameters (figure S1).

Spatial patterns of the RF derived ALT trends exhibit significant variability (figure 5). Globally, about 65% of the NPR showed a deepening ALT trend, with an estimated average NPR-wide deepening trend of 0.11 cm yr^{-1} (25%–75% quantile: [−0.035, 0.204]°cm yr^{-1}). The deepening trends are widespread in some regions such as the Eurasian continent, western Canada and Alaska, and the Qinghai–Tibet plateau. However, there are also areas, such as the Mongolian plateau and northeastern Canada, where a decreasing trend in ALT is observed (figure 5). The RF-derived ALT trend showed significant uncertainties, such that there is a non-significant deepening trend across all latitudes based on the ensemble mean of ALT trend maps. The uncertainties are generally smaller in the high latitude permafrost regions, and higher in the mid-latitude high elevation permafrost regions. Based on the ensemble of 97.5% of ALT trend predictions (high prediction), the ALT is deepening significantly across all latitudes, with a global mean ALT trend of 0.66 cm yr^{-1} (25%–75% quantile: [0.29, 0.81]°cm yr^{-1}). However, based on the ensemble of 2.5% of ALT trend predictions (low predictions), only 12% of the NPR showed a deepening ALT

Figure 4. Spatial patterns of (a) mean, (b) standard deviation, (c) coefficient of variation, and (d) latitudinal gradient summary of mean ALT from 2003 to 2020 by RF methods (colored lines). Permafrost pixel counts within each NPR latitudinal bin denoted by gray bars in plot (d).

trend, averaging -0.43 cm yr^{-1} (25%–75% quantile: $[-0.63, -0.13]°$cm yr^{-1}). It should also be noted that the RF model parameters had a stronger influence on the ALT trend than the spatial sampling bias (figure S2).

3.2. Environmental drivers of ALT mean and trend
Statistical output from the RF models indicated that mean ALT was collectively affected by air and soil temperature, vegetation characteristics, soil properties (such as texture and organic matter content, SM), snow and surface water cover, and topographic properties such as slope and elevation (figure 6). Over the whole NPR, the long-term mean ALT was mostly strongly affected by soil properties, followed by elevation and land-surface temperature. The strong influence of soil properties was consistent with a recent observation-based analysis (Clayton *et al* 2021). Specifically, mean ALT increased with the percent of silt in soil, elevation, SM, LST, SOC, and terrain
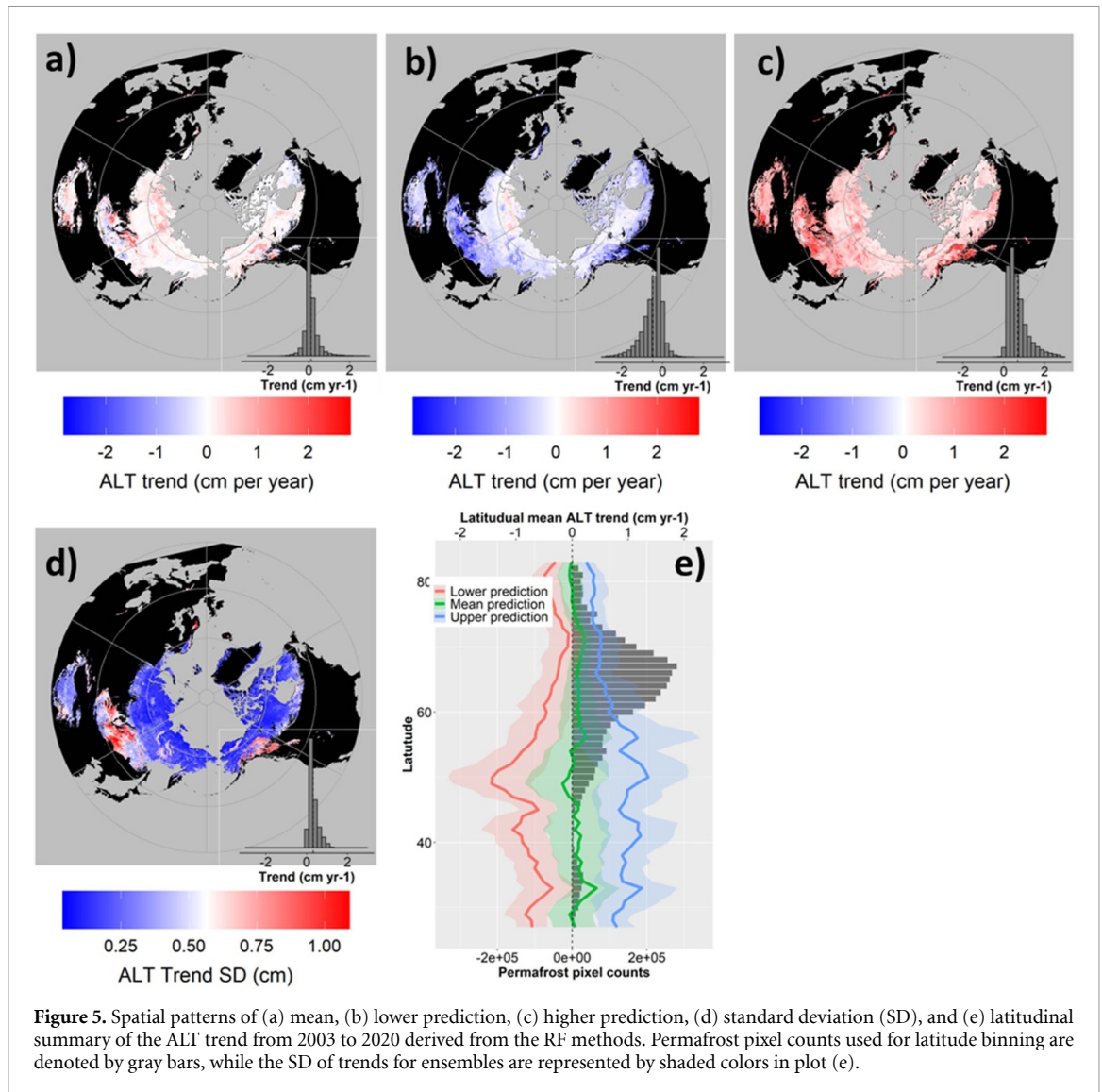
Figure 5. Spatial patterns of (a) mean, (b) lower prediction, (c) higher prediction, (d) standard deviation (SD), and (e) latitudinal summary of the ALT trend from 2003 to 2020 derived from the RF methods. Permafrost pixel counts used for latitude binning are denoted by gray bars, while the SD of trends for ensembles are represented by shaded colors in plot (e).

slope. There was a sharp increase in mean ALT around 1500 m elevation, likely due to the strong influence from high altitude *in situ* measurements in the Qinghai–Tibet and Mongolian plateaus.

Over the NPR, the temporal trend of estimated ALT (2003–2020) was strongly influenced by elevation and the rate of LST change (figure 7). The ALT trends initially decrease at higher elevations up to approximately 1500 m, but then increase at higher altitudes above this elevation threshold. Expectedly, the rate of ALT deepening was positively related to the rate of LST change, and with the timing of seasonal snow cover onset, suggestive of fall warming. Other factors had relatively minor influences on ALT trends.
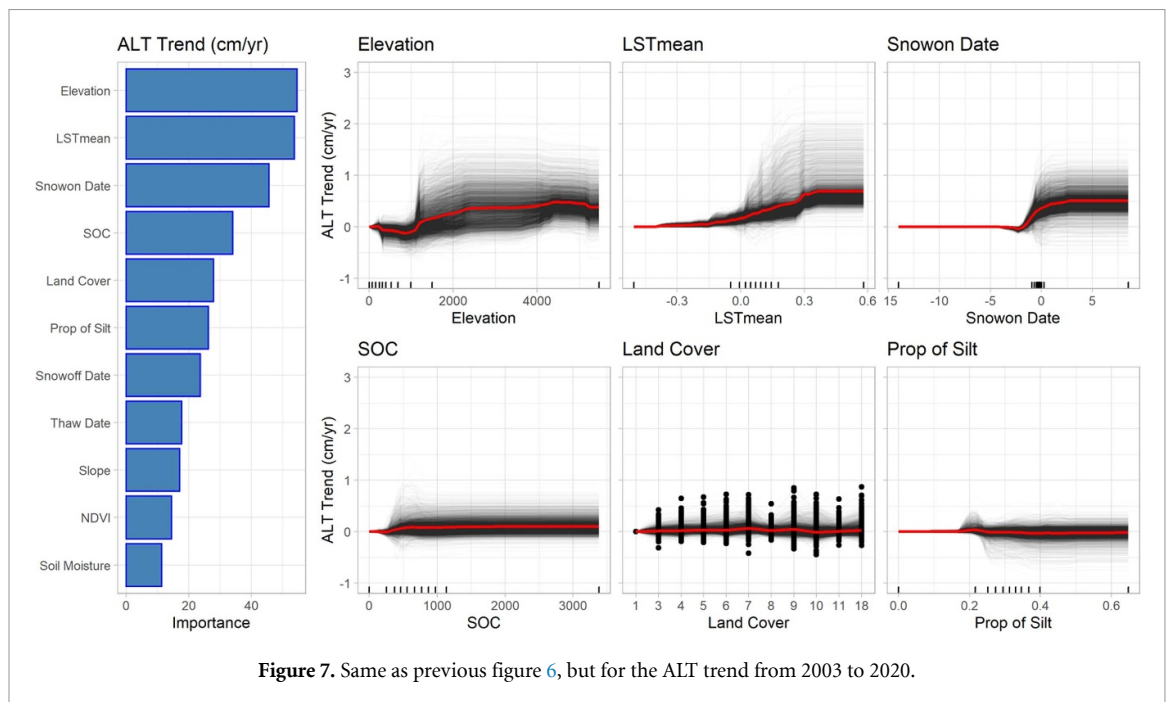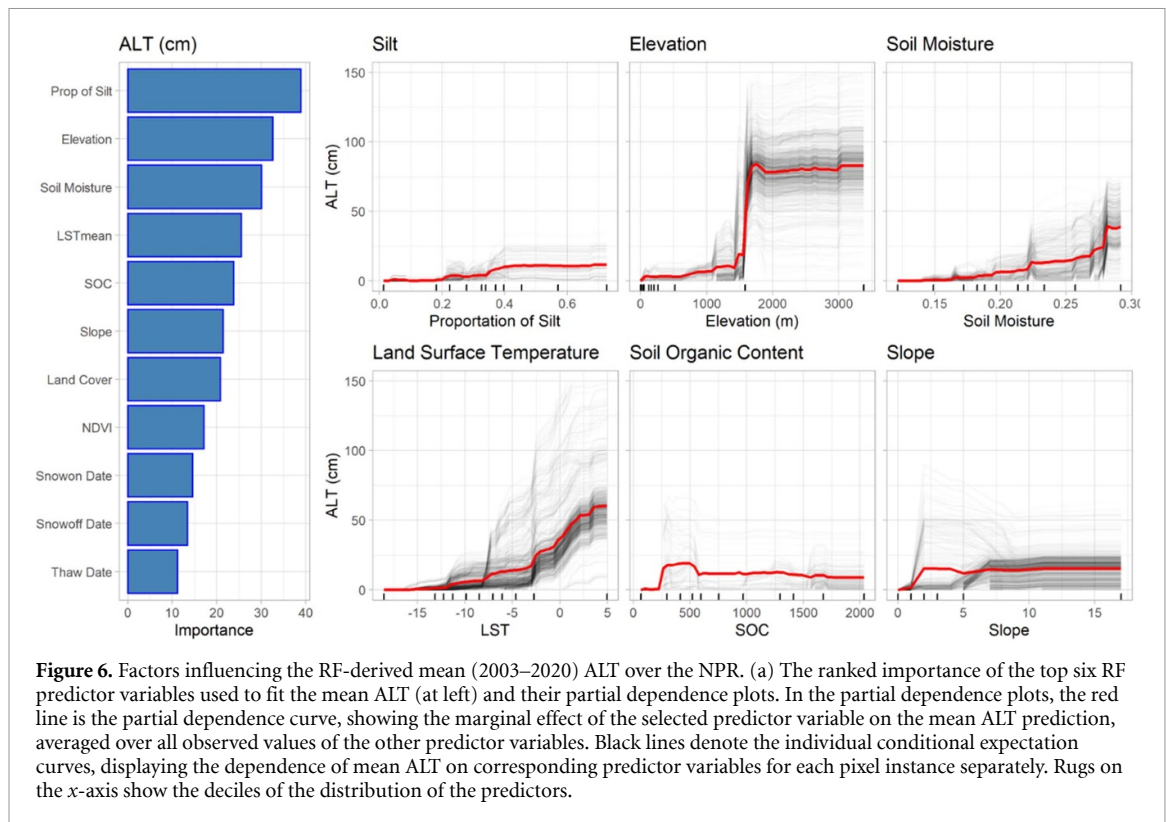
Wildfire can have a significant impact on ALT in permafrost regions due to its effects on surface temperature, vegetation cover and structure, and soil conditions. Generally, our RF predictions suggested a deepening of ALT one-year after fire, with the most pronounced deepening in grasslands (~8 cm) and mixed forests (~5 cm) in the first 1–2 year(s) following a burn event. However, the impact of fire on

ALT quickly disappears after 1–2 years in our mapped product (figure 8). The rapid ALT recovery indicated from the RF predictions is similar to regional process model predictions of ALT recovery from wildfire (Zhang *et al* 2015) and consistent with satellite observations of land surface temperature change after fire (Liu *et al* 2019), but shorter than indicated from field-level measurements, partially due to highly dynamic change in soil and vegetation conditions (Michaelides *et al* 2019).

4. Discussion

4.1. Comparison with other datasets
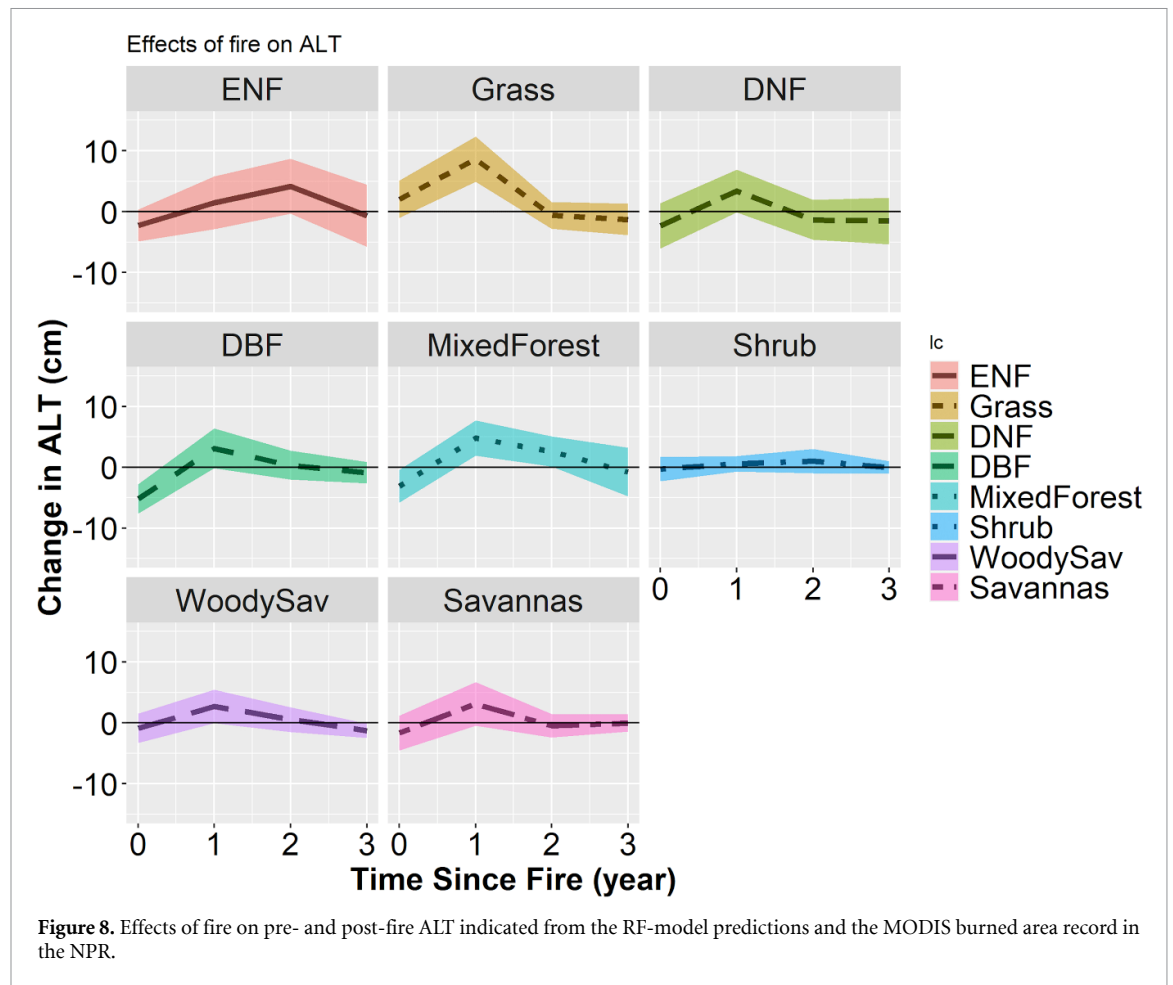
Here we used an ML approach to produce 1°km gridded ALT layers from 2003 to 2020 based on *in situ* ALT network observations and a suite of observational biophysical variables. Compared to the *in-situ* measurements, our gridded ALT data has high accuracy for the mean ALT prediction (RMSE = 21.60 cm, bias = 4.02 cm, $R^2 = 0.97$) and captures the predominant deepening trends (>80%) documented

Figure 6. Factors influencing the RF-derived mean (2003–2020) ALT over the NPR. (a) The ranked importance of the top six RF predictor variables used to fit the mean ALT (at left) and their partial dependence plots. In the partial dependence plots, the red line is the partial dependence curve, showing the marginal effect of the selected predictor variable on the mean ALT prediction, averaged over all observed values of the other predictor variables. Black lines denote the individual conditional expectation curves, displaying the dependence of mean ALT on corresponding predictor variables for each pixel instance separately. Rugs on the *x*-axis show the deciles of the distribution of the predictors.

Figure 7. Same as previous figure 6, but for the ALT trend from 2003 to 2020.

by CALM in recent decades across the NPR. The dataset therefore provides a comprehensive view of landscape level spatial and temporal patterns of ALT over the NPR that corresponds closely with *in situ* ground measurements of ALT represented from the sparse station network. Our results suggest that there are widespread deepening trends of ALT, similar to previous analyses (Park *et al* 2016, Peng *et al* 2018, Li *et al* 2022a, 2022b). Furthermore,

the deepening ALT is broadly aligned with increases in permafrost temperature (Biskaborn *et al* 2019). However, there are significant variations in the rate and pattern of ALT deepening among different studies. Previous studies have suggested the ALT trend ranged from 0.057 ± 0.004 cm yr^{-1} (Peng *et al* 2018) to 0.65 cm yr^{-1} (Li *et al* 2022a) over the NPR. Based on the ensemble of RF-derived ALT predictions, our analysis suggested the ALT increased at a mean rate

Figure 8. Effects of fire on pre- and post-fire ALT indicated from the RF-model predictions and the MODIS burned area record in the NPR.

of 0.11 cm yr^{-1} over the NPR, which is within the range of reported values. The RF-derived ALT dataset showed about 65% of the NPR with a deepening ALT trend, slightly smaller than the value reported by Li *et al* (2022a) (71.17%). Despite uncertainties among studies, these results have unambiguously suggested widespread deepening trends of ALT and permafrost thawing due to climate warming.

At the hemispheric scale, the thermal state and regime of the active layer is primarily dependent on broad climate and permafrost patterns, so that the ALT distribution varies along latitude, altitude and regional permafrost gradients. Accordingly, the variations of ALT are most strongly correlated with near surface air and ground temperatures, especially in summer (Brown *et al* 2000, Luo *et al* 2014). In this sense, the ALT mapping based on thermal index using coarse resolution air temperature could capture the broad-scale variations of past and future change of ALT (Luo *et al* 2014, Park *et al* 2016, Peng *et al* 2018). However, there is a growing need to understand finer landscape-scale change in permafrost states, as this is the scale that is most relevant to ecosystem and hydrological conditions (Heijmans *et al* 2022, Miner *et al* 2022, Smith *et al* 2022). Therefore, our observationally constrained ALT record helps to fill a gap

in understanding finer-scale ALT heterogeneity and control factors across the NPR.

4.2. Environmental controls on ALT

ALT is collectively affected by broad-scale temperature patterns as mediated by elevation and latitude, along with finer landscape level variations in vegetation, soil substrate, micro-relief, and especially SM (Smith *et al* 2022). Therefore, landscape spatial heterogeneity in these factors can either buffer or enhance the impact of top-down climate forcings on ALT trends. As expected, near surface air and ground temperatures have a strong influence on ALT trends, especially affected by the air temperature and its annual amplitude, and the duration of the thaw season (Brown *et al* 2000, Zhang *et al* 2005). Our study also suggested that annual mean land-surface temperature (i.e. LST$_{mean}$) and end of season temperature (i.e. snow on date) have strong influences on ALT trends. Elevation also has a strong influence, consistent with a previous analysis that found ALT in low- and mid-latitude permafrost areas of the Mongolian Plateau and Qinghai–Tibet Plateau having higher rates of ALT deepening (Li *et al* 2022b). Other factors, such as snow cover, vegetation, and soil conditions, also have a strong influence on

ALT. For example, snow cover acts as an insulator, slowing down freeze-thaw cycles in the active layer (Romanovsky and Osterkamp 1997). Vegetation can affect ALT by altering the energy balance at the surface, modifying SM and temperature, and reducing the impact of frost heave (Chen *et al* 2019). Soil properties such as texture, organic matter content, and drainage can affect ALT by influencing the water and heat transfer in the soil. However, the effects of soil properties on ALT may be mediated by other influential factors. The presence of a high water table can cause the active layer to be deeper because of the heat released during the freezing of water. ALT may also be affected by terrain complexity through variations in solar loading and surface energy, and moisture; where steeper slopes tend to have deeper active layers due to increased drainage and reduced snow cover.

Wildfires are a natural disturbance in the NPR, especially in the boreal forest. However, due to a widespread trend toward warmer and drier conditions, larger and more severe fires have been observed, and fire activity is expected to increase further with continued warming (Descals *et al* 2022). These fires damage the protective surface organic layer (Kasischke and Johnstone 2005), which insulates the ground from warm summer air temperatures, decrease the amount of snow interception by trees, reduce the albedo at the ground surface, and lower cooling by evapotranspiration. As a result, ground temperatures and ALT increase following fires, with greater effects observed where burning is more severe and the reduction in the surface organic layer more pronounced. Our RF model captured the deepening ALT trend following fire, but the effects became nearly indistinguishable from undisturbed conditions approximately one or two years after the fire event (figure 8). The unrealistic rapid recovery estimated by the model could be because the RF models only indirectly consider the effects of fire on ALT through changes in vegetation greenness, which tends to have a more rapid post-fire recovery than vegetation structure (Jones *et al* 2013). Therefore, future studies should include other indicators related to changes in soil organic matter and vegetation biomass structure to better capture longer-term effects of fire on ALT (Holloway *et al* 2020).

4.3. Uncertainty and limitations

Although remote sensing techniques are useful in monitoring changes in land-surface indicators associated with permafrost thaw, direct *in situ* measurements of permafrost thermal state or ALT are still required, especially in undersampled regions with high uncertainty. Furthermore, the *in situ* ALT may be biased toward land cover with shallow active layers, because current methods (e.g. probe and ground penetrating radar) are harder to measure ALT with deep active layers. In this analysis, we carefully selected available remote-sensing indicators

related to landscape change associated with permafrost thaw. However, to accurately monitor permafrost degradation, further development of applications that provide direct measurements of important permafrost characteristics are necessary. For instance, improved quantification of ground surface elevation and subsidence, in conjunction with thermal measurements at long-term field monitoring sites, would help establish the extent of permafrost degradation and reconcile measurements of subsidence with displacement measurements from satellite imagery analyses. New applications involving low frequency microwave (L-, P-band) remote sensing offer direct sensitivity to subsurface conditions, including ALT (Michaelides *et al* 2021). Lidar and interferometric synthetic aperture radar sensors can also detect surface deformation trends related to permafrost and active layer conditions (Douglas *et al* 2021, Xu *et al* 2021). These developments offer enhanced capabilities for local to landscape-level monitoring of ALT in the NPR from next generation satellites (Bartsch *et al* 2023) and with less dependence on sparse *in situ* measurement networks.

Another potential limitation in our study concerns the temporal matching of *in situ* data and gridded variables. Most of the *in-situ* data were collected at the end of the growing season when the active layer profile is more likely to be fully thawed. However, the predictors used in our models were summarized at annual or seasonal scales, which may cause a temporal mismatch between ALT and biophysical drivers. Additionally, the inherent limitation of RF modeling, like other statistical or ML approaches, may impact trend estimation. Given the wide range in the spatial distribution of mean annual ALT from centimeters to meters, and the inherent uncertainty of *in situ* ALT measurements used for model training, it is challenging to detect and predict trends in ALT that are often less than 1 cm or mm yr^{-1}. Although RF is powerful in modeling complex variable interactions, it tends to capture the central tendency more than anomalous variations often associated with extreme climate events, leading to an underestimation of spatial and temporal variability, including long-term trends. This may explain why our RF-derived ALT map underestimated the trend compared to CALM measurements. Thus, our newly derived estimates provide a high spatial resolution of mean ALT, but probably provide a conservative estimate of ALT trends.

Our study provides an enhanced landscape (1°km) delineation of ALT trends over the NPR. However, significant ALT heterogeneity occurs at even finer scales on the order of meters (Streletskiy *et al* 2012), and below the effective grain of our model. A possible way to address this issue is to densify the *in-situ* measurements and conduct RF modeling at higher resolution. To demonstrate this, we ran the RF training and analysis using the regionally dense subset of ALT ground observations (~2000 site-years)

located within the NASA ABoVE extended domain (Kasischke *et al* 2010), along with the same set of model inputs. This ABoVE sub-region reanalysis reveals a higher spatial heterogeneity in both the mean and trend of ALT (figure S3). Furthermore, this more regional focused analysis also reveals more subtle controls on the mean and trend of ALT (figures S4 and S5).

5. Conclusion

In this study, we used an ML approach to create 1°km gridded ALT layers from 2003 to 2020 by combining extensive *in situ* ALT observations ($n = 2966$ site-years) with a suite of observational biophysical variables. Our ML-derived ALT record showed high accuracy ($R^2 = 0.97$) and low bias when compared to ALT measurements from sparse NPR monitoring sites. RF analysis revealed that the predicted ALT was primarily influenced by soil properties, followed by elevation and land-surface temperature, which is consistent with previous research (Atchley *et al* 2016). We found a widespread ALT deepening trend over about 65% of the NPR. The ALT has thickened at a mean rate of 0.11 cm yr^{-1} over the NPR in the last two decades. The estimated ALT trends were sensitive to initial fire disturbance impacts represented from satellite derived burned area records even though fire was not directly represented as a model predictor. Our results, together with others, highlight the vulnerability of permafrost to climate warming and other environmental drivers, as well as the widespread deepening in ALT. Our high-resolution ALT data, constrained by observations, provide an updated understanding of the progression of thawing and the thermal state of permafrost in the NPR, and the environmental drivers of these trends. Our open-source dataset provides a high-resolution temporally resolved baseline diagnostic for rapid environmental change that will facilitate other studies and ultimately help advance our understanding of rapid change occurring across the high Arctic.

Data availability statement

All data analyzed in this study are publicly available. MODIS data can be found at LP DAAC (https://lpdaac.usgs.gov/). The ESA soil moisture and permafrost extent data can be found at the ESA Climate Change Initiative website (https://climate.esa.int/en/). Soil data can be found at the soil grid website (https://soilgrids.org/). The dataset can be viewed at https://liuzh833.users.earthengine.app/view/altv1 and downloaded from Zenodo (10.5281/zenodo.10070610).

Conflict of interest

The authors declare to no conflict of interest.

ORCID iDs

Zhihua Liu ⓘ https://orcid.org/0000-0002-0086-5659
Donatella Zona ⓘ https://orcid.org/0000-0002-0003-4839

References

Åkerman H J and Johansson M 2008 Thawing permafrost and thicker active layers in sub-arctic Sweden *Permafr. Periglac. Process.* **19** 279–92

Atchley A L, Coon E T, Painter S L, Harp D R and Wilson C J 2016 Influences and interactions of inundation, peat, and snow on active layer thickness *Geophys. Res. Lett.* **43** 5116–23

Bartsch A, Strozzi T and Nitze I 2023 Permafrost monitoring from space *Surv. Geophys.* **44** https://doi.org/10.1007/s10712-023-09770-31579–613

Berner L T *et al* 2020 Summer warming explains widespread but not uniform greening in the Arctic tundra biome *Nat. Commun.* **11** 4621

Biskaborn B K, Smith S L, Noetzli J, Matthes H, Vieira G, Streletskiy D A, Schoeneich P, Romanovsky V E, Lewkowicz A G and Abramov A 2019 Permafrost is warming at a global scale *Nat. Commun.* **10** 264

Breiman L 2001 Random forests *Mach. Learn.* **45** 5–32

Brown J, Ferrians O J, Heginbottom J A and Melnikov E S 1997 Circum-Arctic map of permafrost and ground-ice conditions

Brown J, Hinkel K M and Nelson F 2000 The circumpolar active layer monitoring (CALM) program: research designs and initial results *Polar Geogr.* **24** 166–258

Chen R H, Tabatabaeenejad A and Moghaddam M 2019 Retrieval of permafrost active layer properties using time-series P-band radar observations *IEEE Trans. Geosci. Remote Sens.* **57** 6037–54

Clayton L K, Schaefer K, Battaglia M J, Bourgeau-Chavez L, Chen J, Chen R H, Chen A, Bakian-Dogaheh K, Grelik S and Jafarov E 2021 Active layer thickness as a function of soil water content *Environ. Res. Lett.* **16** 055028

Descals A, Gaveau D L A, Verger A, Sheil D, Naito D and Peñuelas J 2022 Unprecedented fire activity above the Arctic Circle linked to rising temperatures *Science* **378** 532–7

Douglas T A *et al* 2021 Recent degradation of interior Alaska permafrost mapped with ground surveys, geophysics, deep drilling, and repeat airborne lidar *The Cryosphere* **15** 3555–75

Gorelick N, Hancher M, Dixon M, Ilyushchenko S, Thau D and Moore R 2017 Google Earth Engine: planetary-scale geospatial analysis for everyone *Remote Sens. Environ.* **202** 18–27

Harris C, Arenson L U, Christiansen H H, Etzelmüller B, Frauenfelder R, Gruber S, Haeberli W, Hauck C, Hoelzle M and Humlum O 2009 Permafrost and climate in Europe:

monitoring and modelling thermal, geomorphological and geotechnical responses *Earth Sci. Rev.* **92** 117–71

Harris C, Mühll D V, Isaksen K, Haeberli W, Sollid J L, King L, Holmlund P, Dramis F, Guglielmin M and Palacios D 2003 Warming permafrost in European mountains *Glob. Planet. Change* **39** 215–25

Heijmans M M P D *et al* 2022 Tundra vegetation change and impacts on permafrost *Nat. Rev. Earth Environ.* **3** 68–84

Holloway J E, Lewkowicz A G, Douglas T A, Li X, Turetsky M R, Baltzer J L and Jin H 2020 Impact of wildfire on permafrost landscapes: a review of recent advances and future prospects *Permafr. Periglac. Process.* **31** 371–82

Isaksen K, Sollid J L, Holmlund P and Harris C 2007 Recent warming of mountain permafrost in Svalbard and Scandinavia *J. Geophys. Res.* **112** F02S04

Jones M O, Kimball J S and Jones L A 2013 Satellite microwave detection of boreal forest recovery from the extreme 2004 wildfires in Alaska and Canada *Glob. Change Biol.* **19** 3111–22

Kasischke E S, Goetz S J, Kimball J S and Mack M M 2010 The Arctic-Boreal Vulnerability Experiment (ABoVE): a concise plan for a NASA-sponsored field campaign *Final Report on the VuRSAL/ABoVE Scoping Study*

Kasischke E S and Johnstone J F 2005 Variation in postfire organic layer thickness in a black spruce forest complex in interior Alaska and its effects on soil temperature and moisture *Can. J. For. Res.* **35** 2164–77

LeDell E and Poirier S 2020 H$_2$O AutoML: scalable automatic machine learning *Proc. AutoML Workshop at ICML*

Li C, Wei Y, Liu Y, Li L, Peng L, Chen J, Liu L, Dou T and Wu X 2022a Active layer thickness in the northern hemisphere: changes from 2000 to 2018 and future simulations *J. Geophys. Res.* **127** e2022JD036785

Li G, Zhang M, Pei W, Melnikov A, Khristoforov I, Li R and Yu F 2022b Changes in permafrost extent and active layer thickness in the Northern Hemisphere from 1969 to 2018 *Sci. Total Environ.* **804** 150182

Li X-Y *et al* 2021 Influences of forest fires on the permafrost environment: a review *Adv. Clim. Change Res.* **12** 48–65

Liu Z, Ballantyne A P and Cooper L A 2019 Biophysical feedback of global forest fires on surface temperature *Nat. Commun.* **10** 214

Luo D, Jin H, Jin R, Yang X and Lü L 2014 Spatiotemporal variations of climate warming in northern Northeast China as indicated by freezing and thawing indices *Quat. Int.* **349** 187–95

Luo D, Wu Q, Jin H, Marchenko S S, Lü L and Gao S 2016 Recent changes in the active layer thickness across the northern hemisphere *Environ. Earth Sci.* **75** 555

McGuire A D *et al* 2018 Dependence of the evolution of carbon dynamics in the northern permafrost region on the trajectory of climate change *Proc. Natl Acad. Sci. USA* **115** 3882–7

Michaelides R J *et al* 2021 Permafrost dynamics observatory—part I: postprocessing and calibration methods of UAVSAR L-Band InSAR data for seasonal subsidence estimation *Earth Space Sci.* **8** e2020EA001630

Michaelides R J, Schaefer K, Zebker H A, Parsekian A, Liu L, Chen J, Natali S, Ludwig S and Schaefer S R 2019 Inference of the impact of wildfire on permafrost and active layer thickness in a discontinuous permafrost region using the remotely sensed active layer thickness (ReSALT) algorithm *Environ. Res. Lett.* **14** 035007

Miner K R, Turetsky M R, Malina E, Bartsch A, Tamminen J, McGuire A D, Fix A, Sweeney C, Elder C D and Miller C E 2022 Permafrost carbon emissions in a changing Arctic *Nat. Rev. Earth Environ.* **3** 55–67

Nelson F E, Shiklomanov N I and Nyland K E 2021 Cool, CALM, collected: the circumpolar active layer monitoring program and network *Polar Geogr.* **44** 155–66

Nyland K E, Shiklomanov N I, Streletskiy D A, Nelson F E, Klene A E and Kholodov A L 2021 Long-term Circumpolar

Active Layer Monitoring (CALM) program observations in Northern Alaskan tundra *Polar Geogr.* **44** 167–85

Obu J *et al* 2019 Northern Hemisphere permafrost map based on TTOP modelling for 2000–2016 at 1km^2 scale *Earth Sci. Rev.* **193** 299–316

Obu J 2021 How much of the Earth's surface is underlain by permafrost? *J. Geophys. Res.* **126** e2021JF006123

Obu J, Westermann S, Barboux C, Bartsch A, Delaloye R, Grosse G and Wiesmann A 2021 ESA Permafrost Climate Change Initiative (Permafrost_cci): permafrost active layer thickness for the Northern Hemisphere, v3.0, CEDA (CEDA) (available at: https://catalogue.ceda.ac.uk/uuid/ 67a3f8c8dc914ef99f7f08eb0d997e23)

Park H, Kim Y and Kimball J S 2016 Widespread permafrost vulnerability and soil active layer increases over the high northern latitudes inferred from satellite remote sensing and process model assessments *Remote Sens. Environ.* **175** 349–58

Peng X, Zhang T, Frauenfeld O W, Wang K, Luo D, Cao B, Su H, Jin H and Wu Q 2018 Spatiotemporal changes in active layer thickness under contemporary and projected climate in the Northern Hemisphere *J. Clim.* **31** 251–66

Ran Y *et al* 2022 New high-resolution estimates of the permafrost thermal state and hydrothermal conditions over the Northern Hemisphere *Earth Syst. Sci. Data* **14** 865–84

Romanovsky V E and Osterkamp T E 1997 Thawing of the active layer on the coastal plain of the Alaskan Arctic *Permafr. Periglac. Process.* **8** 1–22

Romanovsky V, Sazonova T, Balobaev V, Shender N and Sergueev D 2007 Past and recent changes in air and permafrost temperatures in eastern Siberia *Glob. Planet. Change* **56** 399–413

Romanovsky V, Smith S, Isaksen K, Shiklomanov N, Streletskiy D, Kholodov A, Christiansen H, Drozdov D, Malkova G and Marchenko S 2019 Terrestrial permafrost [in "State of the Climate in 2018"] *Bull. Am. Meteorol. Soc.* **100** S153–6

Sagi O and Rokach L 2018 Ensemble learning: a survey *Wiley Interdiscip. Rev.* **8** e1249

Schuur E A G *et al* 2022 Permafrost and climate change: carbon cycle feedbacks from the warming Arctic *Annu. Rev. Environ. Resour.* **47** 343–71

Schuur E A *et al* 2015 Climate change and the permafrost carbon feedback *Nature* **520** 171–9

Shiklomanov N, Nelson F, Streletskiy D, Hinkel K and Brown J 2008 The circumpolar active layer monitoring (CALM) program: data collection, management, and dissemination strategies *Proc. 9th Int. Conf. on Permafrost* pp 1647–52

Smith S L, Burgess M M, Riseborough D and Mark Nixon F 2005 Recent trends from Canadian permafrost thermal monitoring network sites *Permafr. Periglac. Process.* **16** 19–30

Smith S L, O'Neill H B, Isaksen K, Noetzli J and Romanovsky V E 2022 The changing thermal state of permafrost *Nat. Rev. Earth Environ.* **3** 10–23

Song X P, Hansen M C, Stehman S V, Potapov P V, Tyukavina A, Vermote E F and Townshend J R 2018 Global land change from 1982 to 2016 *Nature* **560** 639–43

Streletskiy D A, Shiklomanov N I and Nelson F E 2012 Spatial variability of permafrost active-layer thickness under contemporary and projected climate in Northern Alaska *Polar Geogr.* **35** 95–116

Virkkala A M *et al* 2022 The ABCflux database: Arctic–boreal CO$_2$ flux observations and ancillary information aggregated to monthly time steps across terrestrial ecosystems *Earth Syst. Sci. Data* **14** 179–208

Wu Q and Zhang T 2008 Recent permafrost warming on the Qinghai-Tibetan Plateau *J. Geophys. Res.* **113** D13108

Wu T, Xie C, Zhu X, Chen J, Wang W, Li R, Wen A, Wang D, Lou P and Shang C 2022 Permafrost, active layer, and meteorological data (2010–2020) at the Mahan Mountain relict permafrost site of northeastern Qinghai–Tibet Plateau *Earth Syst. Sci. Data* **14** 1257–69

Xu X, Liu L, Schaefer K and Michaelides R 2021 Comparison of surface subsidence measured by airborne and satellite InSAR over permafrost areas near Yellowknife Canada *Earth Space Sci.* **8** e2020EA001631

Zhang T, Frauenfeld O W, Serreze M C, Etringer A, Oelke C, McCreight J, Barry R G, Gilichinsky D, Yang D and Ye H 2005 Spatial and temporal variability in active layer thickness over the Russian Arctic drainage basin *J. Geophys. Res.* **110** D16101

Zhang T, Heginbottom J A, Barry R G and Brown J 2000 Further statistics on the distribution of permafrost and ground ice in the Northern Hemisphere *Polar Geogr.* **24** 126–31

Zhang Y, Wolfe S A, Morse P D, Olthof I and Fraser R H 2015 Spatiotemporal impacts of wildfire and climate warming on permafrost across a subarctic region, Canada *J. Geophys. Res.* **120** 2338–56

Zhao L, Zou D, Hu G, Du E, Pang Q, Xiao Y, Li R, Sheng Y, Wu X and Sun Z 2020 Changing climate and the permafrost environment on the Qinghai–Tibet (Xizang) plateau *Permafr. Periglac. Process.* **31** 396–405

Zhao L, Zou D, Hu G, Wu T, Du E, Liu G, Xiao Y, Li R, Pang Q and Qiao Y 2021 A synthesis dataset of permafrost thermal state for the Qinghai–Tibet (Xizang) Plateau, China *Earth Syst. Sci. Data* **13** 4207–18